Journal of Power Sources 191 (2009) 82–90

Contents lists available at ScienceDirect

Journal of Power Sources

journal homepage: www.elsevier.com/locate/jpowsour

Studies of the pulse charge of lead-acid batteries for photovoltaic applications Part IV. Pulse charge of the negative plate

Angel Kirchev*, Florence Mattera, Elisabeth Lemaire, Kien Dong

Laboratoire des Systèmes Solaires, Institut National de l'Energie Solaire, Commissariat de l'Energie Atomique, 50 avenue du Lac Léman, 73377 Le Bourget du Lac, France

ARTICLE INFO

Article history:
Received 27 August 2008
Received in revised form
26 September 2008
Accepted 27 October 2008
Available online 5 November 2008

Keywords:
Lead acid battery
Negative plate
Pulse charge
Electrochemical impedance spectroscopy
Partial state of charge

ABSTRACT

The paper discusses the influence of the state of charge and pulse charge frequency on the mechanism of the lead-acid battery recharge with pulse current. The data from the pulse charge transients of the negative plate potential at various frequencies show that a decrease of the pulse charge frequency keeping constant average pulse current can impede the charge reaction leading to earlier start of the hydrogen evolution reaction. The dependence of the electrochemical double layer (EDL) capacitance on the state of charge was estimated both during the charge and the discharge using electrochemical impedance spectroscopy measurements at open circuit, followed by equivalent circuit modelling. These data were used to derive the dependence of the average double layer current on SOC and pulse charge frequency. The results show that in the end of the charge almost all of the charge proceeds with the participation of EDL in a certain pulse frequency domain. Using the data from the impedance measurements the optimal pulse charge frequencies were predicted, considering the existence of "electrochemical resonance". The latter appears when the pulse charge frequency approaches the characteristic frequency of the Pb electrodeposition process, given by the product between EDL capacitance and the charge transfer resistance.

1. Introduction

The recent advances in the development of the valve-regulated lead-acid battery (VRLAB) led to several major improvements of the battery performance in comparison with the "classical" flooded design—maintenance-free exploitation due to the operation of internal oxygen cycle, few times longer cycle-life and higher power and energy density due to the use of absorptive glass-mat (AGM) separators [1]. Keeping its low-cost, the VRLA battery became the preferred energy storage system in applications like telecoms, photovoltaic (PV) systems, small electric vehicles (bicycles and scooters), etc.... Recently, several projects of the Advanced Lead-Acid Battery Consortium (ALABC) demonstrated that the VRLA batteries are capable to replace successfully the Ni–metal hydride (Ni–MH) batteries in the hybrid electric vehicles (HEV) [2]. Together with the new benefits from the VRLA design, new problems appeared too. Two of these problems are connected with the charge performance of the negative plate. In the first case, when the efficiency of the oxygen cycle is too high, the negative plate cannot be completely recharged during deep cycling applications typical for the stand alone PV systems and electric vehicles (EV) [3,4]. Thus in the end of the charge the remaining lead sulphate crystals re-crystallize, increasing their size, and the capacity of the negative plate decays due to irreversible sulphation. The second problem appeared when the lead-acid battery was first subjected to the high-rate partial state of charge (HRPSoC) cycling, typical for the hybrid cars [5]. In this case the battery is partially charged and discharged between 40 to 60% SOC, with high-rate pulses with duration 10–60 s due to the regenerative braking, the start and the acceleration assistance functions. It was found that such kind of cycling also leads to premature failure of the negative plates, when usual compositions or designs are used. The main reasons are the presence of surface active substances (most frequently lignosulfonate) as a major part of the expander composition as well as the relatively low surface area of the negative active material (about 10 times lower than the positive active material for the same amount of weight or Amp-hours). A suitable, relatively low-cost solution of these problems can be the use of pulse or intermittent charging current, as it was demonstrated by Nelson et al. [4].

The main aim of this work is to the study the influence of two important parameters—state of charge and pulse current frequency, on the mechanism of the pulse charge of the lead-acid battery negative plate. Since the electrochemical double layer (EDL) is essentially connected with the mechanism of the pulse charge process, an additional aim of this work was to perform a compre-

* Corresponding author. Tel.: +33 4 79 44 45 49.
E-mail address: angel.kirchev@cea.fr (A. Kirchev).

0378-7753/$ – see front matter © 2008 Elsevier B.V. All rights reserved.
doi:10.1016/j.jpowsour.2008.10.098

hensive study of the negative plate impedance in partial state of charge (PSoC).

2. Experimental

2.1. Cells

The experiments were performed on two types of lead-acid cells using battery testing unit SOLARTRON 1470, connected with Frequency Response Analyzer SOLARTRON 1250 for impedance spectroscopy measurements:

- Flooded cell with one 9.0 Ah SLI negative plate (Pb–Ca grid; Vanisperse A as main expander component, thickness 1.45 mm) and two 10 Ah SLI positive plates (Pb–Sn–Ca grid), produced by STECO Power (France), polyethylene separator DARAMIC (Germany), Ag/Ag_2SO_4 reference electrode [6,7], and H_2SO_4 electrolyte with density 1.28 g ml^{-1} (both in the cell and in the reference electrode).
- 10 Ah VRLA cell A502/10 S with gel electrolyte manufactured by EXIDE-Sonnenschein (Portugal), supplied with Ag/Ag_2SO_4 reference electrode. The point of the reference electrode integration was sealed with sealing paste SUN-FIX (Germany).

2.2. Pulse charge characteristics

The general characteristics of the pulse charge were chosen to be close to the ones studied in the previous works focused on the lead-acid battery positive plate [8], i.e. no reverse pulses, pulse cycle ratio $r = t_{ON}/t_{OFF}$ equal to unity, frequency range $f = (t_{ON} + t_{OFF})^{-1}$ between 25 mHz and 50 Hz, where t_{ON} is the half-period during which the charge current with amplitude I_{amp} is applied and t_{OFF} is the rest half-period. The average pulse current which is analogue of the constant charging current can be expressed as $\langle I_p \rangle = r \cdot I_{amp}$; the cells were charged with average current $\langle I_p \rangle$ corresponding to 5 and 10 h rated charge (C_n/5 h and C_n/10 h, where C_n is the nominal capacity of the cell in Ah).

2.3. Impedance spectroscopy measurements

All impedance measurements were performed after 1 h open circuit stay in potentiostatic mode with 5 mV AC amplitude applied over the steady state open circuit potential. The employed AC frequency range was 65 kHz to 10 mHz with a spectral density of 20 points per decade. The equivalent circuit fitting was performed by Z-View2 software.

3. Results and discussion

3.1. The concept of the EDL effect on the mechanism of the charge process

The concept about the connection between the processes of charge and discharge of EDL and the proceeding of electrochemical reactions (charge transfer processes) was initially proposed by Conway et al. in the study of the self-discharge process in supercapacitor electrodes [9,10]. The approach is simple: the EDL is considered as capacitor connected in parallel with one or more electrochemical processes which can be assumed as charge transfer resistors. Thus during the open circuit stay after the interruption of the charge current, the energy stored in EDL can be dissipated by the charge transfer processes, in the current case Pb–metal deposition process. During the pulse charge this loop of charge and self-discharge of EDL is repeated numerous times, depending on the pulse charge frequency, leading to a process obviously different from the constant current charge. The pulse current is frequently used in the electrodeposition technology for the optimisation of different properties of the metal coatings [11].

3.2. Influence of the state of charge on the negative plate potential pulse transients

In order to evaluate the influence of SOC on the pulse charge mechanism the following charge algorithm was applied on the flooded cell: 30 min pulse charge with frequency $f = 1$ Hz, $t_{ON} = t_{OFF} = 0.5$ s, and amplitude $I_{amp} = 3.6$ A (C_n/2.5 h), followed by 1 h open circuit stay and consecutive impedance spectroscopy measurement. The last pulse square-wave was considered to represent the negative plate potential response to the pulse current at the selected state of charge. The loop was repeated 13 times, corresponding to a charge factor $F_{ch} = 130\%$ (the ratio between the injected Amp-hours during the current cycle vs. the discharged Amp-hours during the previous cycle), considering a discharge capacity of 9 Ah. The negative plate potential pulse transients for three different SOC values are presented in Fig. 1. It can be seen that the evolution of the negative plate potential with SOC is completely different from the previously reported data about the positive plate response under the same frequency and pulse current amplitudes [12]. Fig. 1a shows that in the beginning of the charge, EDL is nearly completely charged and self-discharged in the beginning of the "ON" and "OFF" half-period respectively. When the beginning of the hydrogen evolution approaches, the negative plate potential response markedly changes—in the end of the "ON" half-period EDL is not completely charged, while in the end of the following "OFF" half-period the slope $d\varphi/dt$ tends to zero indicating zero capacitive current, hence EDL is completely self-discharged (φ denotes the negative plate potential). In end of the charge (Fig. 1c) during the intensive hydrogen evolution stage, the situation is opposite—EDL is completely charged in the end of the "ON" half-period, but incompletely self-discharged in the end of the "OFF" half-period.

A simple way to characterize quantitatively the pulse charge process further, is to take into account only several "characteristic" points from the negative plate potential pulse transient. These points are shown in Fig. 1a. They correspond to the beginning and the end of the "ON" and "OFF" periods, excluding the ohmic drop effect between the both half-periods. These points can be used to build charge transients of the negative plate potential values vs. the charge time or the injected Amp-hours, as shown in Fig. 2a. The contribution of the EDL in the pulse charge transient can be evaluated by the difference $\Delta\varphi^{ON}$ (shown in Fig. 1c) and $\Delta\varphi^{OFF}$ (shown in Fig. 1b). Both terms are plotted vs. the injected charge in Fig. 2b. The curves of $\Delta\varphi^{ON}$ and $\Delta\varphi^{OFF}$ are nearly identical. They pass a sharp maximum corresponding to the beginning of the active hydrogen evolution stage—the plateau of the $\Delta\varphi_1^{ON}$ and $\Delta\varphi_1^{OFF}$ observed at about −1.5 V. Thus the impact of the EDL on the charge mechanism is strongest in the final third of the charge.

3.3. Influence of the pulse charge frequency on the recharge kinetics

In order to evaluate the influence of the pulse charge frequency on the pulse charge kinetics the VRLA cell was subjected to the following experiment: the cell was charged for 42 min with constant current equal to 1 A, after which it was applied pulse current with various frequencies (starting with the lowest ones) for different duration, keeping the cycle ratio equal to unity ($r = 1$) and the pulse current amplitude equal to 2 A. After the application of the highest frequency the cell was subjected to 6 min constant current polarisation with 1 A, followed by 1 h open circuit stay and an impedance

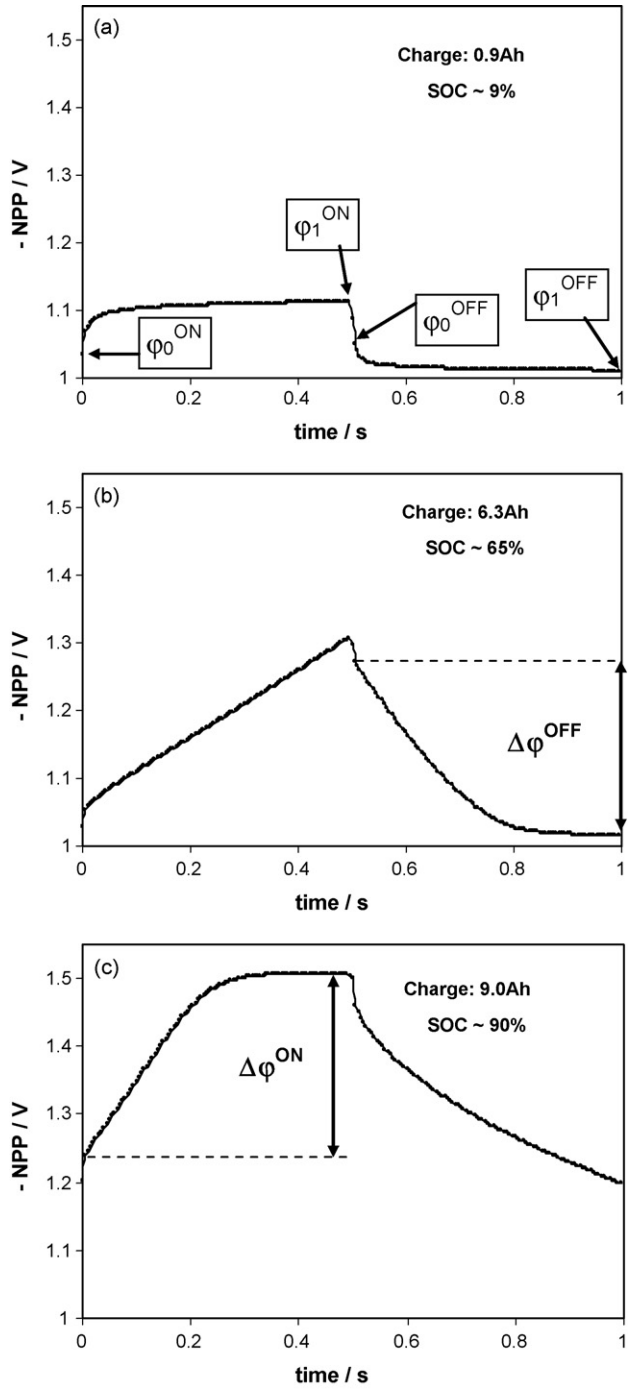

Fig. 1. Negative plate potential transients at state of charge 9% (a), 65% (b) and 90% (c), measured during pulse charge of 9 Ah flooded cell, with pulse current amplitude 3.6 A.

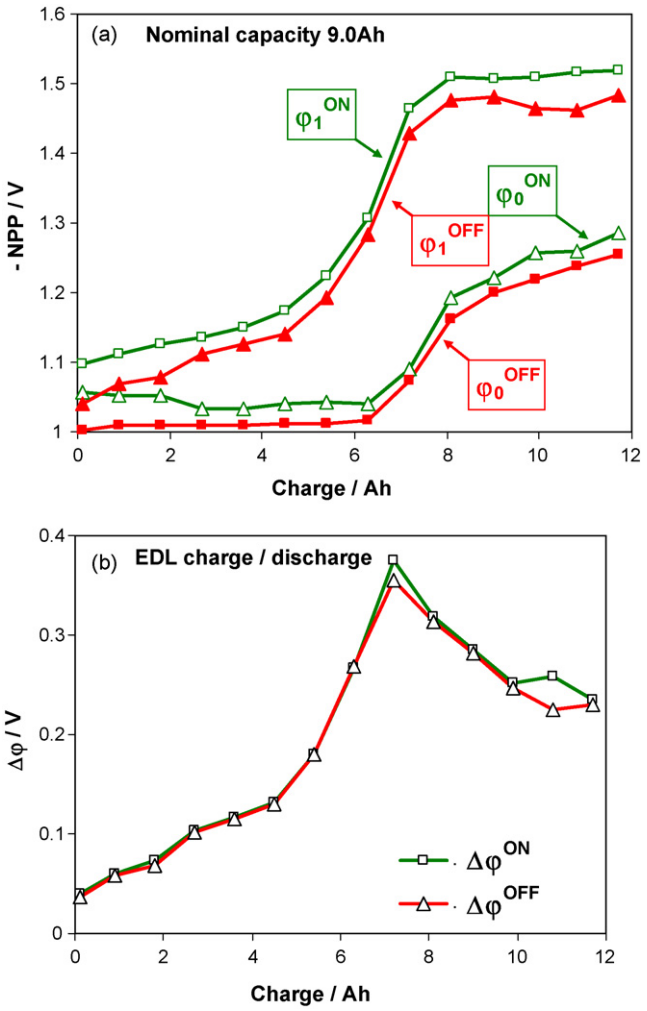

Fig. 2. Evolution of the negative plate potential characteristic points (a) and the potential difference corresponding to the charge and self-discharge of EDL (b) during pulse charge of 9 Ah flooded cell, with pulse current amplitude 3.6 A, frequency 1 Hz and $t_{ON} = t_{OFF}$.

spectroscopy measurement. Each loop corresponds to 10% increase of the SOC. The loop was repeated 8 times (SOC range 0–80%) and its exact description is given in Table 1. The negative plate potential pulse transients for various values of SOC and pulse current frequency are plotted in Fig. 3. The time axis is normalized by multiplication with the pulse current frequency, thus making possible the direct comparison between the transients recorded at different frequencies. The values of the negative plate potential measured during the constant current charge are taken from the end of the 42 min period for point corresponding to the moment $(t \times f) = 0$ and from the beginning of the 6 min period for point corresponding to the moment $(t \times f) = 1$. Fig. 3a shows that in the beginning of the charge (SOC = 19%) the influence of the pulse charge frequency is rather negligible and the average negative plate potential value during the pulse polarisation is quite close to the value corresponding to the constant current charge. At SOC = 50% (Fig. 3b) the influence of the pulse current frequency is already notable—the decrease of the pulse charge frequency increases substantially the charge overvoltage. At SOC = 60% the application of low frequency (50 mHz and 0.5 Hz) pulse current caused an earlier start of the hydrogen evolution process. The pulse charge frequency of 50 mHz corresponds to a period of 20 s, a time interval coinciding roughly to the HRPSoC microcycle typical for HEV. Hence the conversion of the charge current of regenerative braking into series of high-frequency pulses can result in possible improvement in the negative plate partial recharge under HEV cycling.

3.4. Impedance of the negative plate in partial state of charge

The impedance of the $Pb/PbSO_4$ electrode and lead-acid battery negative plate were subject of numerous studies aiming to estimate the fundamental kinetics of the electrode reactions [13–15], the influence of expander materials [16–19], the battery SOC [20],

Table 1
Description of the loop sequence used to study the influence of the pulse charge frequency on the recharge mechanism at constant state of charge.

Loop step index	Frequency [Hz]	Time [s]	Number of pulses
1		42 min/constant current/1 A	
2	0.025	200 s	5
3	0.05	100 s	10
4	0.5	40 s	20
5	1	20 s	20
6	5	4 s	20
7	10	2 s	20
8	20	1 s	20
9	50	0.2 s	20
10		6 min/constant current/1 A	
11		60 min open circuit stay	
12		Impedance spectroscopy	

the changes in the negative active material porosity [21–24], the influence of the electrolyte gelling [25,26] or negative plate failure mode under fast charge cycling [27]. The equivalent circuit modelling of the negative plate impedance has been discussed recently in the PhD thesis of Karden [28], where three time constant model (two capacitive and one pseudo-inductive time constants) is proposed without further detailed discussion on the nature of the time constants.

The impedance characterisation of the negative plate in partial state of charge is necessary in order to quantify the data about the effect of the EDL on the pulse charge mechanism. The EIS measurements were carried out in the SOC interval 0–100% both in charge and in discharge direction, for each 10% change in SOC. The main aim of this impedance study is to estimate the EDL capacitance using the equivalent circuit approach combined with Differential Impedance Analysis (DIA) [29,30]. The method of DIA performs a numerical treatment of the impedance spectrum, providing useful information about the number of time constants, number and approximate values of the resistive and capacitive components in the studied system prior to its representation and modelling using equivalent circuit hypothesis. The method of DIA was recently successfully applied in the fuel cell research [31–38] as well as in the characterisation of the lead-acid battery positive plate in partial state of charge [39]. The output of DIA is the AC frequency distribution of the Local Operation Model (LOM) parameters—the effective resistance $R_{\text{eff}}(\omega)$, representing different charge transfer components of the impedance, the effective capacitance $C_{\text{eff}}(\omega)$, representing the presence of dielectric or semi-conductive components in the system (EDL, passivation or adsorption layers, etc.. . .), and the additional resistance $R_{\text{add}}(\omega)$ which is analogue of the different components of the ohmic series resistance of the systems. The LOM structure represents the model of a simple Faradic process: R_{eff} is connected in parallel with C_{eff}, and in series with R_{add}.

3.4.1. Differential impedance analysis and equivalent circuit modelling of the lead-acid battery negative plate in partial state of charge

Fig. 4 shows both Nyquist and DIA temporal plots of the negative plate impedance for three different SOC values during the charge. The high-frequency "tail" ($\omega > 500$–600 Hz) can be related to the inductance of the cables and current collectors. The shape of the capacitive part ($Z'' < 0$) of all Nyquist plots suggest that the number of the time constants in the system is at least two. In most of the spectra a third time constant can be suggested too. The application of DIA makes possible the further recognition of the number of the time constants, respectively the rate limiting processes in the negative plate electrochemistry.

At low SOC values the frequency distribution of the effective resistance $R_{\text{eff}}(\omega)$ can be divided in three frequency domains, where two plateaus can be seen in domains I and II, and rather distributed part is situated in domain III. The frequency distribution of the effective capacitance $C_{\text{eff}}(\omega)$ can be also set in the same three frequency domains, as well as the distribution of the effective time constant $T_{\text{eff}}(\omega)$. An important feature of the $C_{\text{eff}}(\omega)$ function is the absence of flat parts (plateaus), which means that the capacitive elements in the system (EDL capacitance for example) are frequency distributed [29], i.e. they could be modelled as Constant Phase Elements (CPE) with the corresponding impedance:

$$Z_{\text{CPE}} = T^{-1}(\mathrm{j}\omega)^{-P} \tag{1}$$

where T and P are the CPE empiric parameters and $\mathrm{j} = (-1)^{1/2}$ is the imaginary unit.

The shape of the $R_{\text{eff}}(\omega)$, $C_{\text{eff}}(\omega)$ and $T_{\text{eff}}(\omega)$ curves remains almost same during the entire charge in domains I and II. However at low frequencies ($\omega < 0.1$ Hz) the general character of the $R_{\text{eff}}(\omega)$, $C_{\text{eff}}(\omega)$ and $T_{\text{eff}}(\omega)$ curves changes dramatically, indicating that at different SOC values and at different direction of the negative plate polarisation (φ_i^- values from the Nyquist plots correspond to the negative plate potential prior to the current switching off) the nature of the rate limiting process is different.

At SOC values close to 50% (Fig. 4b and e) the low-frequency domain III is depressed down to a narrow frequency band. In some of the measured spectra in the same frequency band it was observed also a small pseudo-inductive loop. Such low-frequency pseudo-inductive loops measured in galvanostatic-controlled mode are reported by Karden [28] for negative plates in industrial lead-acid batteries.

In the end of the charge after the start of the intensive hydrogen evolution ($\varphi_i^- = -1.509$ V) all three domains are again apparent in the DIA plot (Fig. 4f), while in the Nyquist plot the beginning of the third semicircuit is just suggested (Fig. 4c).

In order to explain the nature of the different time constants it is necessary to discuss the electrochemistry and structure of the negative plate. The conversion of the lead sulphate into lead and vice versa proceeds via "dissolution/precipitation" model, which is slightly modified by the presence of the expander, usually a lignosulfonate derivative. The expander molecules form adsorption layers [40] on the lead and lead sulphate surface, which stabilize the wetting film between these two solid phases [41]. So the surface area of the interface metal (Pb)/electrolyte (thin liquid film) remains unaffected by the formation of $PbSO_4$ crystals, and the discharge capacity is maintained high during the cycling. But the same adsorption layer on the Pb surface also increases substantially the charge polarisation, i.e. the transfer of the Pb^{2+} from the electrolyte in the NAM pore into the outer Helmholtz layer of EDL. Hence the "dissolution/precipitation" model can be expressed by the following equations:

$$PbSO_4 + H^+ \Leftrightarrow {Pb_{pore}}^{2+} + {HSO_4}^- \tag{2a}$$

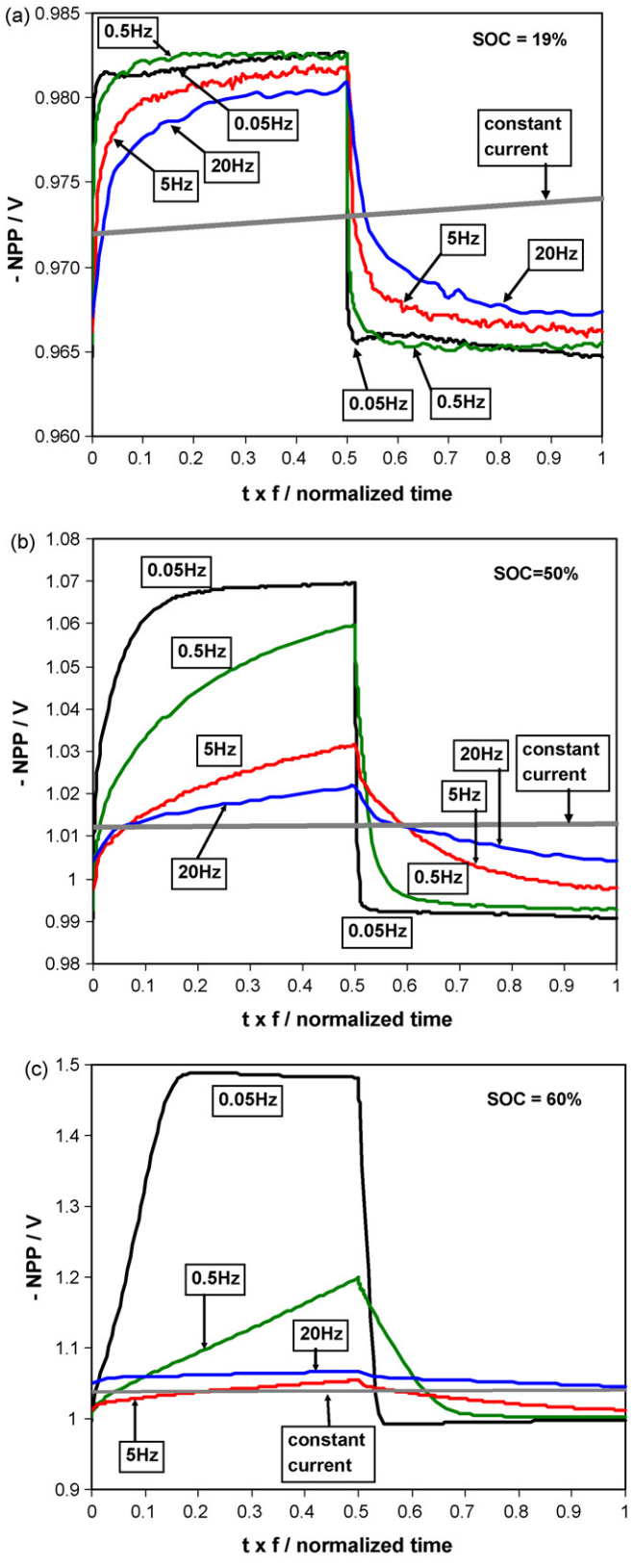

Fig. 3. Negative plate potential transients at state of charge 19% (a), 50% (b) and 60% (c), measured during charge of 10 Ah VRLA (gel) cell, with various pulse frequencies and current amplitude equal to 2 A.

$$Pb_{pore}{}^{2+} \Leftrightarrow Pb_{EDL}{}^{2+} \quad (2b)$$

$$Pb^{2+} + 2e^{-} \Leftrightarrow Pb \quad (2c)$$

Eq. (2a) represents a diffusion controlled process, which should be observed as Warburg impedance at low frequencies—a straight line in the Nyquist plot with 45° slope. In the present study no Warburg-type of impedance has been observed down to 10 mHz, thus the reaction (2a) can be considered as a fast process at PSoC. Eq. (2c) is fast electrochemical reaction and it can be regarded as a simple Faradic process, giving the main contribution to the high frequency impedance of the negative plate. Its equivalent circuit representation is charge transfer resistance R_{ct} in parallel with the double layer capacitance C_{dl}. The process denoted with reaction (2b) can be considered as charge (ion) transfer through adsorption layer, and its equivalent circuit representation is again a resistor (adsorption resistance R_{ads}) in parallel with a capacitor (adsorption capacitance C_{ads}). Since the processes (2a)–(2c) are consecutive, both RC circuits should be connected is series, as it is shown in Fig. 4a–c. The fitting with this equivalent circuit gives very good results for frequencies as low as 50 mHz both for partially charged and partially discharged negative plate in wide SOC range: from 10 to 90%.

But how can be explained the evolution of the low-frequency impedance of the negative plate considering the processes taking place during the charge and the discharge? At low SOC values the quantity of the lead sulphate in the NAM pores is substantial. In this case the ionic current in the pore can be hindered. Since the lead sulphate is an insulator, this hindrance can cause the appearance of the third loop in the low frequency part of the impedance spectrum.

In the SOC range 30–60% the third loop is very depressed and can be neglected, but above SOC = 60% it appears again. The "size" of this loop increases with the increase of the difference between the open circuit potential and the negative plate potential under charge polarisation. In this SOC range the hydrogen evolution begins and takes place together with the lead sulphate reduction. Hence, substantial part of the lead surface can be occupied by adsorbed H-atoms and the third loop in the impedance spectra in the end of the charge can be related to the adsorption of hydrogen.

Because of the complexity of the phenomena related to the low-frequency impedance of the negative plate impedance and since this study is focused on the pulse charge and participation of EDL in it, the employed equivalent circuit will include only two time constants.

3.4.2. Evolution of the equivalent circuit parameters with SOC during the charge and the discharge of the negative plate

After the Z-View2 fitting, both capacitive constant phase elements (CPE_{dl} and CPE_{ads}) were converted into pure capacitors according to the procedure proposed by Hsu and Manfred [42]. The obtained dependences of R_{ct}, C_{dl}, R_{ads} and C_{ads} are plotted in Fig. 5. The ohmic resistance R_{ohm} from the equivalent circuit is nearly constant in SOC range 10–90%. At SOC equal to 0 and 100% R_{ohm} was found about 20% higher in comparison with the observed plateau between SOC = 10% and SOC = 90%, probably due to the formation of dense $PbSO_4$ layer in the end of the discharge and the presence of some hydrogen bubbles in the NAM pores at the end of the charge.

Fig. 5a shows that during the charge the capacity of the double layer increases nearly linearly with SOC, as predicted theoretically and measured by other methods [43], due to the increase of the electro-active surface, reaching nearly constant value in the end of the charge. The further fluctuations of C_{dl} values in the end of the charge could be related to the adsorption of H-atoms. However, during the discharge the dependence of EDL capacity on SOC is quite different: in a very wide SOC range C_{dl} remains nearly constant,

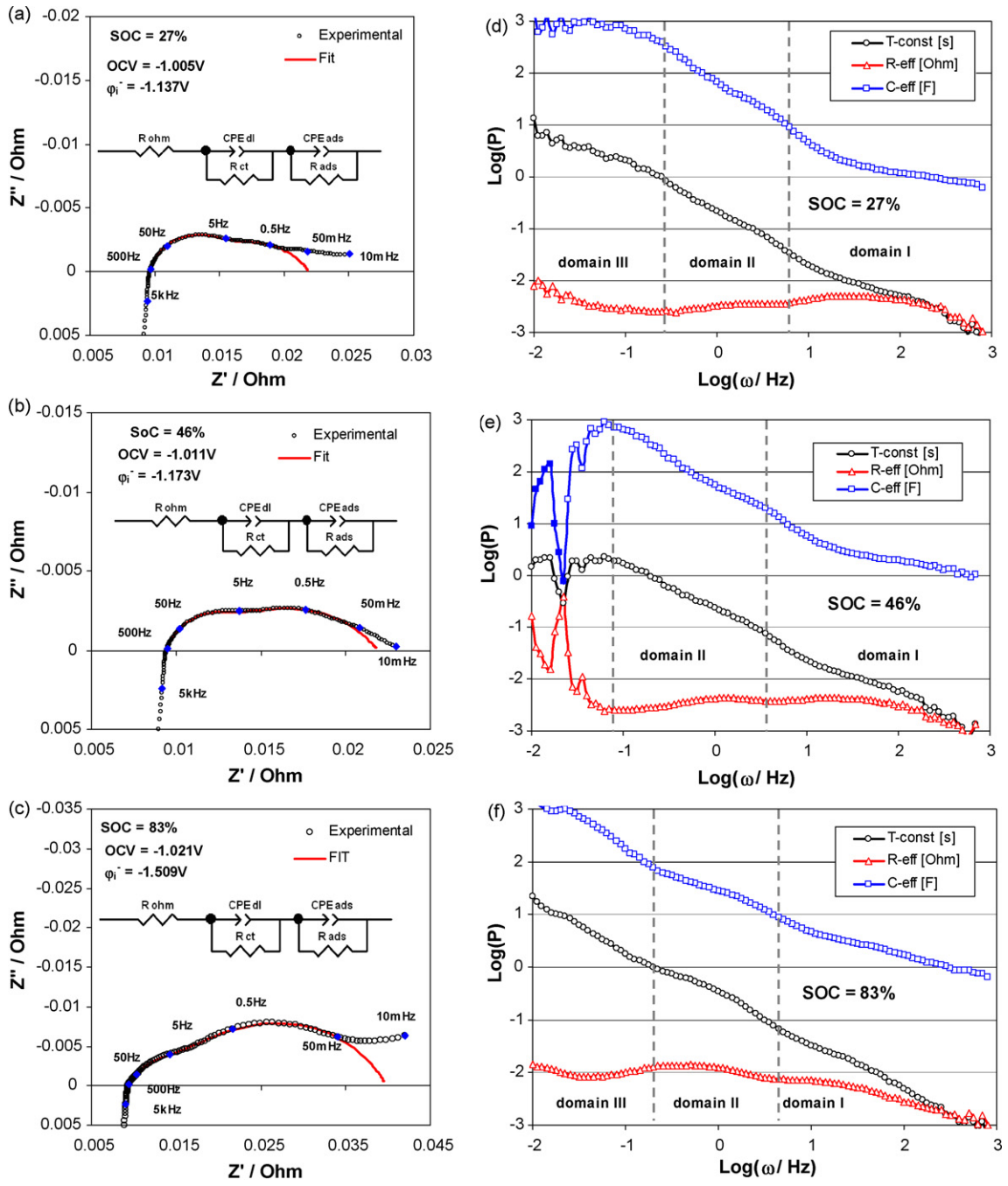

Fig. 4. Evolution of the negative plate impedance during the pulse charge of 9 Ah flooded cell.

and below SOC value 20–30%, C_{dl} drops rapidly tending to zero for completely discharged plate. This huge hysteresis can be related to the presence of the adsorption layer of expander molecules on the lead surface: since the Pb^{2+} transfer through the expander layer is limited, it is expected that during the discharge the quantity of the Pb^{2+} in the space between the metal surface and the adsorption layer (i.e. in the EDL) will be higher keeping the same value of SOC. The capacitance of Helmholtz type of EDL is proportional to the surface density of the charge according to formula:

$$C_{dl} = \frac{dq}{dV} \tag{3}$$

where "dq" is the variation of the surface density of the charge and "dV" is the change of the electric potential across the EDL. During the discharge the lead surface area decreases. In the same time "dq" can increase due to the "trapping effect" of the expander on the Pb^{2+} ions. These two opposite effects can keep C_{dl} value constant if they are from the same order of magnitude.

The above-raised hypothesis can explain also the hysteresis between the R_{ct}(SOC) and C_{ads}(SOC) curves obtained for the charge and for the discharge, shown in Fig. 5b and c. The charge transfer resistance curve is markedly shifted to lower values in the whole SOC interval. This parameter is connected with the exchange current I_0 of the reaction (2c) as follows:

$$R_{ct} = \frac{RT}{I_0 F} \tag{4}$$

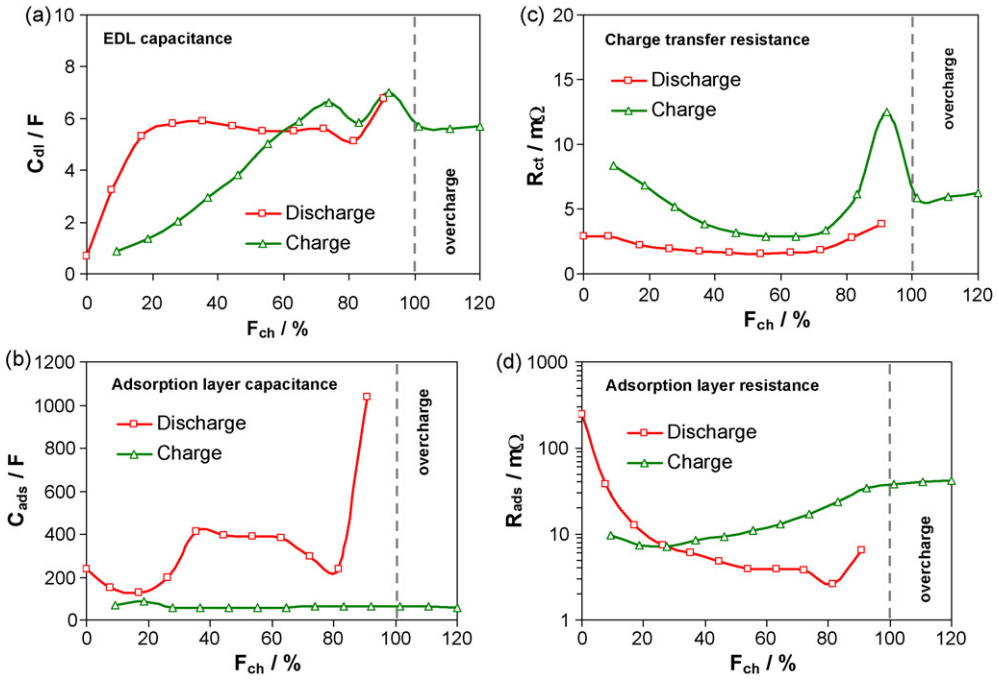

Fig. 5. Dependence of EDL capacitance (a), charge transfer resistance (b), adsorption capacitance (c) and adsorption resistance (d) on the quantity of the injected charge expressed as a charge factor. The data are for 9 Ah flooded cell.

where R is molar gas constant, T is the temperature and F is the Faraday's constant. On the other hand the exchange current is proportional to the surface concentration of the species participating in the electrochemical reaction, i.e. the lead (II) ions. Thus lower R_{ct} values correspond to higher Pb^{2+} local concentration at the lead surface.

The capacitance of the adsorption layer C_{ads}(SOC) shown in Fig. 5c is also shifted to higher values during the entire discharge. Again this hysteresis can be explained by the accumulation of Pb^{2+} ions between the metal surface and the adsorption layer and corresponding increase of the surface charge density in the adsorption capacitor C_{ads}.

The retention of Pb^{2+} ions in the space between the lead surface and the layer formed by adsorbed lignosulfonate molecules was demonstrated recently be Hirai et al. [44] using *in situ* Atomic Force Microscopy (AFM) and cyclic voltammetry—the AFM images are taken for each 10 mV during sweeps with rate 10 mV s^{-1}. It was clearly demonstrated that the lead sulphate crystals appear on the electrode surface after the maximum of the anodic peak corresponding to the discharge reaction of Pb dissolution and $PbSO_4$ precipitation.

The adsorption resistance R_{ads} plotted vs. SOC in Fig. 5d can be related to the thickness of the adsorption layer. In the end of the discharge R_{ads} increases markedly, suggesting the formation of two or more adsorption layers on the lead surface.

3.5. *Influence of the state of charge on the average double layer current*

The average double layer current $\langle I_{dl}\rangle$ was proposed recently as a simple parameter evaluating the participation of EDL in the electrochemical reactions taking place during pulse current polarisation [12]. For pulses with cycle ratio $r = 1$ the average double layer current is equal to:

$$\langle I_{dl}\rangle_{OFF} = 2fC_{dl}(\varphi_1^{OFF} - \varphi_0^{OFF}) \quad \text{and} \quad \langle I_{dl}\rangle_{ON} = 2fC_{dl}(\varphi_1^{ON} - \varphi_0^{ON}) \quad (5)$$

Appling Eq. (5) to the data shown in Figs. 2b and 5a, the plots of the average double layer current vs. the injected Amp-hours were built. The corresponding data is shown in Fig. 6. The average pulse current increases markedly and after the start of the hydrogen evolution it exceeds the pulse current amplitude. The main reason for this contradiction is the difference between the measured steady state values of the double layer capacitance used in Eq. (5) and the dynamic C_{dl} values during the pulse charge. In the end of the pulse charge the applied overvoltage is 300–500 mV vs. the open circuit potential of the electrode $Pb/PbSO_4$ and there is intensive hydrogen evolution causing substantial adsorption of H-atoms. Both factors can alter the values of C_{dl} in comparison with open circuit ones. No matter of this contradiction, it can be seen that the impact of the pulse charge is highest in the final stages of the charge, a result sim-

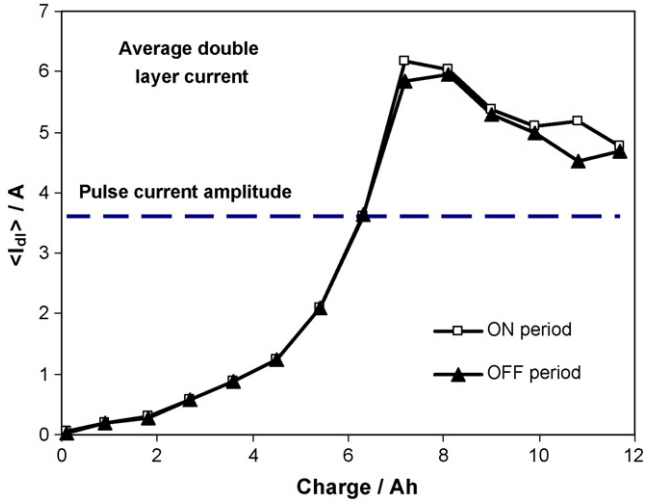

Fig. 6. Dependence of the average double layer current on the quantity of the injected charge. The data are for 9 Ah flooded cell, charged with pulse current amplitude 3.6 A, frequency 1 Hz and $t_{ON} = t_{OFF}$.

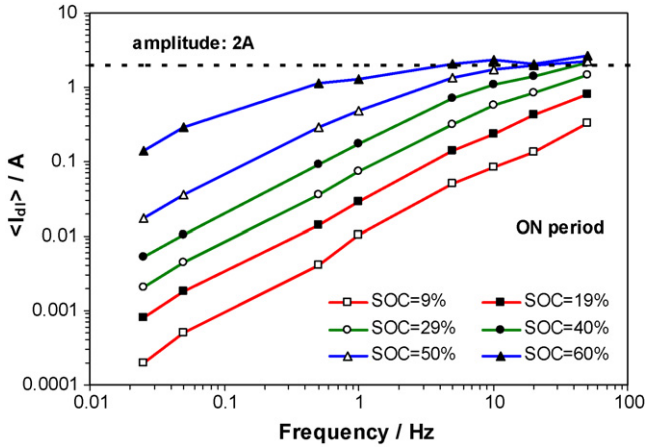

Fig. 7. Dependence of the average double layer current on the pulse charge frequency. The data are for 10 Ah VRLA (gel) cell. The pulse current amplitude is 2 A and $t_{ON} = t_{OFF}$.

ilar to the one observed previously at the lead-acid battery positive plate [12].

3.6. Influence of the pulse frequency on the average double layer current

The data shown in Fig. 3 together with the corresponding impedance measurements were used to obtain the dependence of the average pulse current for various SoC values. The result is plotted in Fig. 7. It can be seen that in the beginning of the charge $\langle I_{dl} \rangle$ is nearly a linear function of the frequency in the studied domain. However in the further stages of the charge (SOC ~40–60%) the $\langle I_{dl} \rangle$ tends to the pulse amplitude. From the theoretical point of view, in wide enough pulse frequency range the curves in Fig. 7 should exhibit a maximum. Since the pulse charge is a periodic perturbation over a given object with its own certain characteristic frequency, the maximum of $\langle I_{dl} \rangle$ will have the meaning of electrochemical resonance maximum. Using the equivalent circuit approach it is obvious that the characteristic frequency of the charge reaction (2c), is proportional to $(R_{ct}C_{dl})^{-1}$. It expected that close to the resonance frequency the charge acceptance would be maximal. The dependence of the characteristic frequency $(R_{ct}C_{dl})^{-1}$ as a function of SOC is given in Fig. 8. The data show that pulse charge with frequency about 50 Hz would be optimal for HRPSoC cycling, while frequency about 20–30 Hz are rather suitable for deep cycling applications in order to facilitate the complete charge of the negative plate. It should be noted that these frequencies are more than one order of magnitude higher than the optimal frequencies for pulse charge of the positive plate recharge. This means that the pulse charge frequency can "target" the optimisation of the electrode with more critical performance. The results from Fig. 8 explain also the "depolarizing" effect of the high-frequency current shown in Fig. 3b and c: when the frequency increases it approaches the characteristic frequency for the given SOC value increasing the charge acceptance.

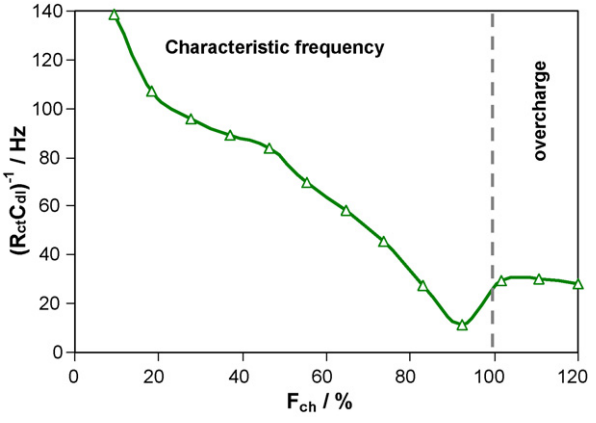

Fig. 8. Dependence of the characteristic frequency of the Pb electrodeposition process on the quantity of the injected charge.

4. Conclusions

The application of pulse current during the charge of the negative plate alters most substantially the reaction mechanism in the final stages of the recharge. In this case almost all of the current is redirected via EDL, i.e. during the "ON" period of the pulse square wave EDL is charged, and during the subsequent "OFF" period EDL is self discharged by the charge transfer process of $PbSO_4$ reduction or hydrogen evolution at more negative plate potentials. The EDL capacitance on the negative plate was studied be EIS during the charge, the overcharge and the discharge. The application of DIA on the measured impedance spectra indicated the presence of three time constants in the equivalent circuit of the negative plate. The high (5–500 Hz) and medium (0.5–5 Hz) frequency time constants correspond to the electrochemical reaction of lead electrodeposition/electrodissolution and the subsequent impeded transfer of Pb^{2+} ions through the adsorption layer of lignosulfonate macromolecules formed on the Pb surface. The same adsorption layer causes hysteresis in the curves of the equivalent circuit parameters in charge and in discharge direction. Only the ohmic resistance did not exhibit hysteresis behaviour—its value remains constant in the SOC range 10–90% both in charge and in discharge direction. The results from the impedance experiments provided the dependence of the characteristic frequency of the lead electrodeposition/electrodissolution process on SOC. This frequency gives the optimal pulse charge frequency. Thus the phenomenon, which can be categorized as "electrochemical resonance", will result in maximum charge acceptance when the pulse current has frequency coinciding with the characteristic frequency of the charge transfer process of the lead (II) reduction. Since the adsorption of the expander limits substantially the charge current it can be concluded that an increase of the pulse cycle ratio towards 0.8–0.9 can increase further the charge acceptance because in this way the pulse current amplitude will be markedly lower and closer to the average pulse charge current.

Acknowledgements

The financial support of this work has been provided by E.ON International Research Initiative, as a part of the project "Benefits of Storage Systems for Stationary Grid-Connected and Advanced Vehicle Applications" (BEST).

References

[1] P.T. Moseley, D.A.J. Rand, in: D.A.J. Rand, P.T. Moseley, J. Garche, C.D. Parker (Eds.), The Valve-regulated Battery - A Paradigm Shift in Lead-Acid Technology, Elsevier, Amsterdam, 2004, pp. 479–481 (Chapter 1).
[2] A. Cooper, M. Kellaway, L. Lam, J. Furukawa, B. Wahlqvist, Proceedings of the Advanced Automotive Battery Conference, Tampa, FL, May 2008.
[3] R.H. Newnham, in: D.A.J. Rand, P.T. Moseley, J. Garche, C.D. Parker (Eds.), Remote-Area Power Supply (RAPS) Systems and the Valve-Regulated Lead-Acid Battery, Elsevier, Amsterdam, 2004, pp. 479–481 (Chapter 14).
[4] R.F. Nelson, E.D. Sexton, J.B. Olson, M. Keyser, A. Pesaran, J. Power Sources 88 (2000) 44.
[5] P. Moseley, J. Power Sources 127 (2004) 27–32.

[6] P. Ruetschi, J. Power Sources 113 (2003) 363–370.
[7] P. Ruetschi, J. Power Sources 116 (2003) 53–60.
[8] D. Benchetrite, M. Le Gall, O. Bach, M. Perrin, F. Mattera, J. Power Sources 144 (2005) 346–351.
[9] B.E. Conway, J. Electrochem. Soc. 138 (1991) 1539–1548.
[10] J. Niu, B.E. Conway, W.G. Pell, J. Power Sources 135 (2004) 332–343.
[11] M.S. Chandrasekar, Malathy Pushpavanam, Electrochim. Acta 53 (2008) 3313.
[12] A. Kirchev, M. Perrin, E. Lemaire, F. Karoui, F. Mattera, J. Power Sources 177 (2008) 217–225.
[13] K.V. Rybalka, E.M. Strochkova, Sov. Electrochem. 13 (1977) 1148–1152.
[14] A.N. Fleming, J.A. Harrison, J.M. Ponsford, Electrochim. Acta 22 (1977) 1371–1374.
[15] Min Ma, Chun-Xiao Yang, Wen-Bin Cai, Wei-Fang Zhou, Hou-Tian Liu, J. Electrochem. Soc. 150 (2003) B325–B328.
[16] M.P.J. Brennan, N.A. Hampson, J. Electroanal. Chem. Interface Electrochem. 54 (1974) 263–268.
[17] E.M. Strochkova, K.V. Rybalka, Sov. Electrochem. 13 (1977) 62–65.
[18] M. Saakes, P.J. van Duin, A.C.P. Ligtvoet, D. Schmal, J. Power Sources 47 (1993) 129–147.
[19] C. Francia, M. Maja, P. Spinelli, J. Power Sources 95 (2001) 119–124.
[20] G. Lindbergh, Electrochim. Acta 42 (1997) 1239–1246.
[21] L.A. Beketaeva, K.V. Rybalka, Sov. Electrochem. 23 (1986) 342–346.
[22] K.V. Rybalka, L.A. Beketaeva, Sov. Electrochem. 23 (1987) 389–392.
[23] K.V. Rybalka, L.A. Beketaeva, J. Power Sources 30 (1990) 269–273.
[24] L.A. Beketaeva, K.V. Rybalka, J. Power Sources 32 (1990) 143–150.
[25] M.P. Vinod, K. Vijayamohanan, J. Power Sources 89 (2000) 88–92.
[26] L. Wu, H.Y. Chen, X. Jiang, J. Power Sources 107 (2002) 162–166.
[27] G. Petkova, D. Pavlov, The mechanism of failure of the negative plate in lead-acid battery on fast charging, Bulg. Chem. Commun. 36 (2004) 61–65.
[28] E. Karden, Using Low-frequency Impedance Spectroscopy for Characterization, Monitoring, and Modeling of Industrial Batteries, Ph.D. thesis, Shaker Publishing, Aachen, 2002.
[29] Z. Stoynov, D. Vladikova, Differential Impedance Analysis, Prof. Marin Drinov Academic Publishing House, Sofia, 2005.
[30] Z. Stoynov, Electrochim. Acta 34 (1989) 1187–1192.
[31] D. Vladikova, Z. Stoynov, M. Viviani, J. Eur. Ceram. Soc. 24 (2004) 1121–1127.
[32] D. Vladikova, G. Raikova, Z. Stoynov, H. Takenouti, J. Kilner, St. Skinner, Solid State Ionics 176 (2005) 2005–2009.
[33] A. Barbucci, P. Carpanese, M. Viviani, P. Piccardo, D. Vladikova, Z. Stoynov, Proceedings of the 1st European Fuel Cell Technology and Applications Conference, 2005, p. 109.
[34] D. Vladikova, J.A. Kilner, S.J. Skinner, G. Raikova, Z. Stoynov, Electrochim. Acta 51 (2006) 1611–1621.
[35] A. Barbucci, M. Viviani, P. Carpanese, D. Vladikova, Z. Stoynov, Electrochim. Acta 51 (2006) 1641–1650.
[36] M. Cabeza, P. Merino, A. Miranda, X.R. Nóvoa, I. Sanchez, Cement Concrete Res. 32 (2002) 881–891.
[37] M.P. Carpanese, G. Cerisola, M. Viviani, P. Piccardo, D. Vladikova, Z. Stoynov, A. Barbucci, J. Fuel Cell Sci. Tech. 5 (2008) (art. no. 011010).
[38] D.E. Vladikova, Z.B. Stoynov, A. Barbucci, M. Viviani, P. Carpanese, J.A. Kilner, S.J. Skinner, R. Rudkin, Electochim. Acta 53 (2008) 7491–7499.
[39] A. Kirchev, A. Delaille, M. Perrin, E. Lemaire, F. Mattera, J. Power Sources 170 (2007) 495–512.
[40] B.O. Myrvold, J. Power Sources 117 (2003) 187.
[41] D. Pavlov, in: B.D. McNicol, D.A.J. Rand (Eds.), Power Sources for Electric Vehicles, Elsevier, Amsterdam, 1984, pp. 135–137.
[42] C.H. Hsu, F. Mansfeld, Corrosion 57 (2001) 747–748.
[43] D.H.J. Baert, A.A.K. Vervaet, A new method for the measurement of the double layer capacitance for the estimation of battery capacity, The 25th International Telecommunications Energy Conference, INTELEC'03, 19–23 Oct. 2003, pp. 733–738.
[44] N. Hirai, Y. Kimura, H. Vermesan, S. Kubo, K. Magara, Proceedings of the 7th International Conference on Lead-Acid Batteries LABAT 2008, 9–12 June, 2008, Varna, Bulgaria, 2008, p. 175.